Int J CARS (2013) 8:877–885
DOI 10.1007/s11548-012-0800-8

ORIGINAL ARTICLE

Automated measurement of mandibular cortical width on dental panoramic radiographs

Chisako Muramatsu · Takuya Matsumoto · Tatsuro Hayashi · Takeshi Hara · Akitoshi Katsumata · Xiangrong Zhou · Yukihiro Iida · Masato Matsuoka · Takashi Wakisaka · Hiroshi Fujita

Received: 16 August 2012 / Accepted: 5 November 2012 / Published online: 23 November 2012

Abstract
Purpose Mandibular cortical width (MCW) measured on dental panoramic radiographs (DPRs) was significantly correlated with bone mineral density. We developed a computer-aided diagnosis scheme that automatically measures MCW to assist dentists in describing a possible osteoporotic risk and suggesting further examinations.
Methods In our approach, potential mandible edges are detected by modified Canny edge detector. On the basis of the edge information, a contour model is selected from the reference data and is fitted to the test case by using the active contour model. The reference mental foramina positions of the model are employed as the MCW measurement locations. The MCW is measured on the basis of the grayscale profiles obtained along the lines perpendicular to the fitted mandible contour. One hundred DPRs, including 26 DPRs from osteoporotic cases, were used to evaluate our proposed scheme.
Results Experimental results showed that the average MCWs for osteoporotic and control cases were 2.2 and 3.9 mm, respectively. When a threshold of 2.7 mm was applied, the sensitivity and specificity for identifying osteoporotic patients were 88.5 and 97.3 %, respectively.
Conclusion An automated MCW measurement technique is feasible using DPRs, and this method has a potential to identify asymptomatic osteoporotic patients.

Keywords Osteoporosis · Dental panoramic radiography · Computer-aided diagnosis · Mandibular cortical width · Active contour model

C. Muramatsu (✉) · T. Matsumoto · T. Hayashi · T. Hara · X. Zhou · H. Fujita
Department of Intelligent Image Information, Graduate School of Medicine, Gifu University, 1-1 Yanagido, Gifu 501-1194, Japan
e-mail: chisa@fjt.info.gifu-u.ac.jp

A. Katsumata · Y. Iida · M. Matsuoka · T. Wakisaka
Department of Oral Radiology, School of Dentistry, Asahi University, 1851 Hozumi, Mizuho, Gifu 501-0296, Japan

Present address:
T. Matsumoto
NTT Communications, 1-1-6 Uchisaiwaicho, Chiyoda-ku, Tokyo 100-8019, Japan

Present address:
T. Hayashi
Media Co., Ltd, 3-26-6 Hongo, Bunkyo-ku, Tokyo 113-0033, Japan

Introduction

Two hundred million or more patients are suffering from osteoporotic diseases all over the world [1]. Because the osteoporotic disease rate increases with age [2], the number of patients is expected to increase in aging countries, such as Japan. Due to the asymptomatic nature of osteoporosis, bone strength is gradually weakened unnoticeably. As a result, a small force in daily workload can bring fractures of the femur and hip bones, which may cause elders to be bedridden and degrade their quality of life. Osteoporotic fractures represent a huge public health burden and incremental medical costs. Therefore, it is important to detect and treat osteoporosis early. For the diagnosis of osteoporosis, dual energy X-ray absorptiometry (DXA) is often used. However, because of the asymptomatic nature of osteoporosis and the availability of DXA at large medical facilities, only small number of people receives DXA examinations.

It has been found that mandibular cortical width (MCW) on a dental panoramic radiograph (DPR) is significantly correlated with bone mineral density (BMD) in the hip, lumbar spine, and foramen, so that the MCW measurement is effective for osteoporosis screening [3–5]. DPRs are used to examine dental diseases in dental clinics over the world; especially, in the United States, United Kingdom, and Japan, more than 17, 1.5, and 10 million DPRs, respectively, are taken annually in dental clinics [3]. Identifying asymptomatic patients with osteoporosis through dental examinations may bring a supplemental benefit to the patients. However, most DPRs were used only for diagnosing dental conditions by dentists in their routine clinical work.

In recent years, there is an apparent interest in studies on the measurement of MCW on DPRs. Figure 1 shows a DPR with an enlarged view of the cortical bone under the mental foramen (MF) where MCW is generally measured in clinical studies. Computer-aided diagnosis (CAD) system that quantitatively measures MCW on DPRs may be useful for dentists to identify asymptomatic patients with osteoporosis at an early stage. Arifin et al. [6] proposed a CAD system for measuring MCW by identifying the cortical margin on the basis of the gradient analysis. When the method was applied to 100 DPRs, the results indicated a potential usefulness of this method for identifying the postmenopausal women with low skeletal BMD. However, their system required the manual assistance in determining the MF positions and selecting two points on cortical margin. In their subsequent study [7], the cortical margin was determined automatically by use of various image processing techniques; however, the regions of interest around the MF were identified manually.

Allen et al. [8] proposed a computerized method for measuring MCW without and with manual intervention by detecting upper and lower cortical edges between the MF and antegonion separately on the right and left sides using an active shape model (ASM). In the semiautomated mode, an expert provided four reference points on the lower mandible edge at the right and left MF and antegonion. Although the lower edge detection was relatively successful in both modes, lateral misalignment can occur in the automated mode, resulting in MCW measurement different from the reference anatomical positions. In their subsequent study, Roberts et al. [9,10] proposed a hybrid method combining the ASM and an active appearance model to improve the reliability of automatic search. This method achieved comparable accuracy to the previous semiautomated method; however, they reported about 10–25 % failure or inadequacy on more challenging dataset, in which manual initialization was later applied.

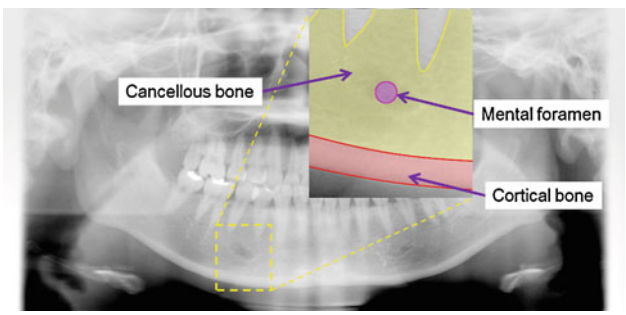

Fig. 1 Dental panoramic radiograph and the enlarged view near the mental foramen

We propose a computerized scheme for automatically measuring MCW on DPRs. Some of our preliminary investigation results have been reported in [11]. The uniqueness of the proposed scheme is that our fully automated scheme utilizes a mandibular contour model, which is selected from the reference cases on the basis of the similarity to a test case. The reference models contain manually determined mandibular contour and the MF positions. The contour of the selected model is then fitted to the test case using active contour model (ACM), and the fitted reference MF points were employed for MCW measurement. By applying the single-line model for the right and left sides and using the reference MF points, mislocalization of the measurement positions may be reduced. In addition, the model was applied only to the lower mandibular edge, where edge is more apparent, and the endocortical margin was determined by the profile analysis.

Materials and methods

DPR database

Our preliminary study database consists of a hundred DPRs obtained at Asahi University Hospital, Gifu, Japan, and was used for developing and testing our computerized scheme. These DPRs were originally obtained for the purpose of examining dental diseases, except for 17 normal volunteers. The consecutive DPR cases were retrospectively collected if the patient had a history of having a DXA examination at Asahi University Hospital. The research protocol was approved by the institutional review boards at Asahi University and Gifu University. Out of the 83 clinical cases, 26 of them have been diagnosed with osteoporosis on the basis of DXA examination. The cases include 35 males and 59 females with the average ages of 53 and 57, respectively ($p = 0.4$); the age and/or gender information were missing in 6 patients and could not be retrieved because of our IRB policy of image anonymization without traceability. The DPRs were imaged with Veraview Epocs (J. Morita MFG. Corp., Kyoto, Japan) and CR 75.0 (Agfa, 2Mortsel, Belgium). The images are in Digital Imaging and Communications in Medicine (DICOM) format with 1,420 × 2,920 pixels, 0.1 mm pixel resolution, and 12-bits grayscale. Because of the limited number of cases available, they were used for training and testing our scheme by using a leave-one-out test method.

MCW measurement scheme

Detection of MF, which is often located under the mandibular second premolar in adults, can be difficult because of the low contrast of MF on DPRs and a lack of teeth in some elders. Therefore, our system utilizes the mandibular contour model and determines the measurement locations. At these locations, MCWs are measured on the basis of intensity profiles along the lines perpendicular to the mandibular contour. The overview of our proposed scheme consisting of three steps is illustrated in Fig. 2 with an example in each step. The three steps are as follows:

- Step 1: Detection of potential mandibular edges by using mandibular mask and modified Canny edge detector
- Step 2: Selection of a reference contour model and fitting of the model by ACM
- Step 3: Measurement of MCWs based on the grayscale profile analysis along the lines perpendicular to the mandibular contour

The details of our proposed scheme are described below.

Preparation of the mandibular mask

For the detection of reliable lower mandibular edges, a mandibular mask was used. The description of the usage will be described in the following sections. For each DPR, lower mandibular margin was manually delineated by a coauthor (T.M.) under the guidance of the dental radiologist (A.K.). These 100 manual contours were aligned, and by applying the morphologic operation, the combined region was dilated with a circular element with 100 pixels in diameter, resulting in the mandibular mask shown in upper right of Fig. 2. To detect edges with specific directions, the mask was divided into 7 subregions by drawing the lines from the middle point of the upper mask edge in the directions of 35, 45, 75, 105, 115, and 145 degrees. The mask with the 7 subregions $R = \{R_1, R_2, R_3, \ldots R_7\}$ is shown in Fig. 2, which was employed in the edge detection process using the modified Canny edge detector.

Mandibular edge detection

In step 1, potential lower mandibular edges were detected in order to select the most similar reference contour model in the next step.

To reduce patients' dose, DPRs are generally obtained with low radiation exposure leaving the high quantum noise. Therefore, the Canny edge detector [12] was employed to smooth out high frequency noise and select reliable edges. The edge detection by the Canny edge detector consists of image smoothing, determination of edge strengths and directions, non-maximal edge suppression, and hysteresis thresholding.

First, for reducing the noise, image smoothing was carried out by using the Gaussian filter. In this study, a standard deviation of the Gaussian function was set to 0.3 mm. In general, the Canny edge detector utilizes the Sobel operator for the determination of edge strengths and directions. However, by applying the Sobel filter to a whole image, many edge components unrelated to the mandible would be detected. In DPR, locations of mandibular edges can be limited and the direction of the edges can be predicted by the prior knowledge. Therefore, we utilized the mandibular mask image (Fig. 2) as a template for the Canny edge detector as in Kirsch's method [13].

By taking into account the shape of the mandibular bone, expected directions of the contour edges in the subregions of the mask can be determined, such as the vertical edges in regions R_1 and R_7, and horizontal edges in region R_4. On the basis of these prior knowledge, the edge strength, $f_2(i, j)$, in each subregion, was defined as

$$f_2(i,j) = \begin{cases} \sum_{x=-1}^{1}\sum_{y=-1}^{1} g_{xy}^{(1)} \cdot f(i+x, j+y), & \text{if } f(i,j) \in R_1 \\ \max_{z=1,2}\sum_{x=-1}^{1}\sum_{y=-1}^{1} g_{xy}^{(z)} \cdot f(i+x, j+y), & \text{if } f(i,j) \in R_2 \\ \sum_{x=-1}^{1}\sum_{y=-1}^{1} g_{xy}^{(2)} \cdot f(i+x, j+y), & \text{if } f(i,j) \in R_3 \\ \sum_{x=-1}^{1}\sum_{y=-1}^{1} g_{xy}^{(3)} \cdot f(i+x, j+y), & \text{if } f(i,j) \in R_4 \\ \sum_{x=-1}^{1}\sum_{y=-1}^{1} g_{xy}^{(4)} \cdot f(i+x, j+y), & \text{if } f(i,j) \in R_5 \\ \max_{z=4,5}\sum_{x=-1}^{1}\sum_{y=-1}^{1} g_{xy}^{(z)} \cdot f(i+x, j+y), & \text{if } f(i,j) \in R_6 \\ \sum_{x=-1}^{1}\sum_{y=-1}^{1} g_{xy}^{(5)} \cdot f(i+x, j+y), & \text{if } f(i,j) \in R_7 \\ 0, & \text{otherwise} \end{cases} \quad (1)$$

where g_{xy} are the direction kernels and are expressed as follow.

$$g^{(1)} = \begin{bmatrix} -3 & -3 & +5 \\ -3 & 0 & +5 \\ -3 & -3 & +5 \end{bmatrix} \quad g^{(2)} = \begin{bmatrix} -3 & +5 & +5 \\ -3 & 0 & +5 \\ -3 & -3 & -3 \end{bmatrix}$$

$$g^{(3)} = \begin{bmatrix} +5 & +5 & +5 \\ -3 & 0 & -3 \\ -3 & -3 & -3 \end{bmatrix} \quad g^{(4)} = \begin{bmatrix} +5 & +5 & -3 \\ +5 & 0 & -3 \\ -3 & -3 & -3 \end{bmatrix} \quad (2)$$

$$g^{(5)} = \begin{bmatrix} +5 & -3 & -3 \\ +5 & 0 & -3 \\ +5 & -3 & -3 \end{bmatrix}$$

The vertical edges (R_1 : 270°, R_7 : 90°) were detected in R_1 and R_7, either the vertical (R_2 : 270°, R_6 : 90°) or the diagonal (R_2 : 135°, R_6 : 45°) edges with the maximum strength were employed in R_2 and R_6, the diagonal edges (R_3 : 135°, R_5 : 45°) were detected in R_3 and R_5, and the horizontal edges (R_4 : 0°) were detected in R_4.

The edge components detected by using the mask were thinned by a non-maximal edge suppression algorithm. This algorithm compares the edge strength of a pixel in question

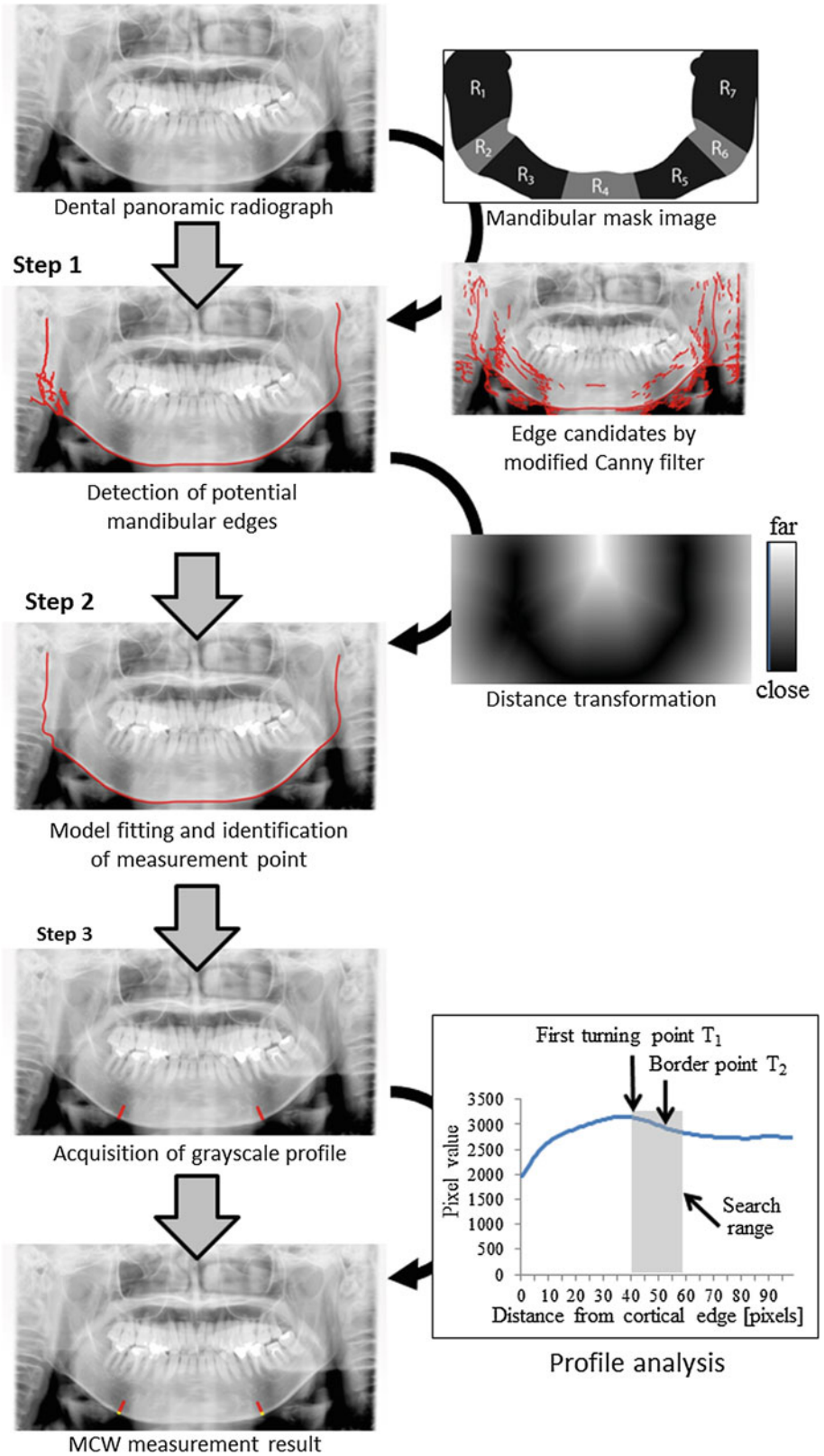

Fig. 2 Overview of our proposed method for measuring MCW. Output for each step is shown in the *left column*, and images and a plot in the *right column* describe the intermediate processing

with those of the neighbor pixels and removes the pixel from the edge candidates if it is lower than those of the neighbors. Finally, the edges were detected by the hysteresis thresholding. This technique employs two threshold values, T_h and T_l, corresponding to the high and low values, respectively. Pixels with the edge strength above T_h were determined as edge

components, those below T_l were determined as non-edge components, and those between were considered edge components only if they were connected with the edge components. In this study, $T_l = 100$ and $T_h = 1{,}000$ were employed which were determined empirically. In Fig. 2 below the mandibular mask, the result of applying the modified Canny edge detector based on the prior knowledge is shown. It can be seen that many unrelated edges were removed.

For further removing the false edges, the most probable edge in each subregion was retained. Edges detected in the regions around the mandibular angles (R_2 and R_6) and the center, right-end, and left-end regions (R_4, R_7, and R_1) of DPRs can include the edges of the mandibular angle on the opposite side and the cervical vertebrae. On the other hand, the mandibular edges can be detected relatively reliably in large pieces around the regions below the mental foramina (R_3 and R_5). The vertical posterior edges in R_1 and R_7 may be detected dependably if the overlap with the vertebrae is small. Therefore, the longest horizontal edges in R_3 and R_5 and the longest vertical edges in R_1 and R_7 were retained, and other edges in these subregions were removed. In other regions, the edge that was closest to the selected ones in the neighbor regions, R_1, R_3, R_5, and R_7, was selected. The final edge components remained by the above procedure are shown in Fig. 2 (step 1). At this point, some false edges might be detected; however, they did not strongly affect the subsequent process.

Selection of a reference contour model and fitting of the model by ACM

An accurate delineation of the mandibular contour and determination of MF positions are important for the measurement of MCW. In the second step, the lower border of the mandible was determined using the reference contour model and fitting it by ACM [14].

The manual mandibular contours obtained earlier comprised the reference models, each of which also contained the reference points corresponding to the right and left MF locations identified by the dental radiologist. In the leave-one-out testing, the model corresponding to the test case was removed and the reference model was selected from the remaining 99 models.

Figure 3 shows the flowchart of the mandibular contour determination process. First, distance transformation was applied to the potential edge image obtained in the previous step. The resulted image has the pixel values representing the Euclidean distance from the nearest contour edge. In Fig. 2, the distance images obtained by applying the distance transformation to the edge detection results (step 1) is shown. Using this distance image, the most similar reference contour model was selected. For the similarity measure, each reference model was overlaid to the distance image of a test

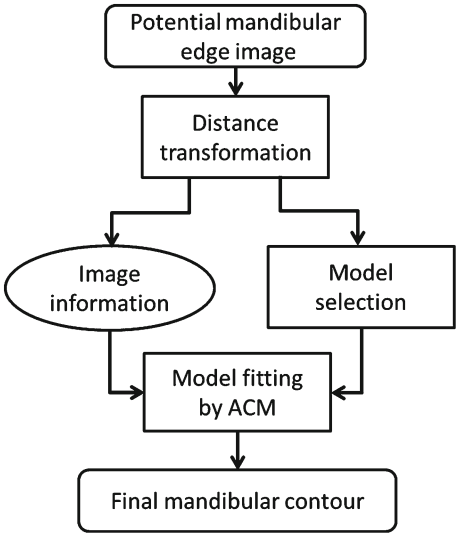

Fig. 3 A flowchart of mandibular contour determination process using the reference model and ACM

case and the average distance of the pixels overlapped with the reference contour pixels was determined. The reference image with the smallest average distance was selected, and its manual contour was used for the initial control points in the model fitting by the ACM.

In the general ACM, the gradient information based on the derivative of the original pixel values is used for adjusting the contour. However, in DPRs, the use of gradient information is not suitable because the cervical vertebrae are next to the contour edges, and the posterior edges of the mandible are not effectively enhanced. Therefore, in the proposed method, the distance image was employed for fitting the contour.

The contour optimization is proceeded by iteratively adjusting a set of control points on the closed curves, $v(s) = (x(s), y(s))$, $s \in [0, 1]$, to minimize the following energy function.

$$E_{\text{snake}} = E_{\text{int}}(v) + E_{\text{image}}(v) \tag{3}$$

$$E_{\text{int}} = \frac{1}{2}\int_0^1 \alpha \left|\frac{\partial v}{\partial s}\right|^2 + \beta \left|\frac{\partial^2 v}{\partial s^2}\right| \mathrm{d}s \tag{4}$$

$$E_{\text{image}} = \int_0^1 P(v(s))\,\mathrm{d}s \tag{5}$$

$$P(x, y) = -\gamma \cdot \text{dist}\,(\text{mask}\,([G_\sigma \otimes I(x, y)])) \tag{6}$$

The parameters α, β, and γ are the weighing coefficients which were set to $\alpha = 0.2$, $\beta = 0.2$, and $\gamma = 0.6$ in this study. $P(x, y)$ is the probability of the contour passing the pixel. G_σ represents the Gaussian filter, and *mask* and *dist* correspond to the edge detection process using the mask and the distance transformation, respectively. In this study, the end points of the contour model were connected to obtain

the closed curve, and the control points were placed in every 5 mm along the contour model. The adjustment of the control points was made only in the radial direction as specified for edge detection using the mandibular mask. The termination condition was either that no control point was moved or the number of iterations exceeded 200 times. When the adjustment was completed, a smooth contour was determined by the spline interpolation. The mandibular contours determined by fitting the selected model by ACM are shown in Fig. 2 (step 2). The results show that the mandibular contours can be determined as single curves.

Based on the edge detection result shown in Fig. 2 (step 1), it seems that the model fitting may not be necessary for determining the mandibular contour; however, by applying the reference contour model, the mandibular contour can be determined in a single smooth curve and the MCW measurement positions can be reliably located. When the ACM was applied, the control points that were closest to the reference MF points of the selected model were identified. After the control points were fitted to a test case, the locations of the corresponding MF points were selected as the measurement positions.

Measurement of MCW by the grayscale profile analysis

In the third step, MCW was measured on each of the right and left MF positions by the profile analysis.

For increasing the reliability of the measurement, 21 profiles were obtained on and around the right and left measurement positions along the contour. At each profile acquisition pixel, a first-degree approximation function $f(x) = ax + b$ for the mandibular contour was determined by the least squared method with 21 contour points. The parameters a and b were determined by

$$a = \frac{N\sum xy - \sum x \sum y}{N\sum x^2 - \left(\sum x\right)^2} \tag{7}$$

$$b = \frac{\sum x^2 \sum y - \sum xy \sum x}{N\sum x^2 - \left(\sum x\right)^2} \tag{8}$$

where N corresponds to the number of sampling points, which was 21. Using the above function, a pixel value profile along the perpendicular line was obtained, and the border point between the cortical bone and trabecular bone was determined. The number of sampling points on the profile was set to 100 pixels in this study.

In Fig. 2, the lower right plot shows a grayscale profile along a perpendicular line. It generally takes the form that the pixel value first increases, and at some point, it stays constant or starts decreasing. This point can be considered as the border of the cortical and trabecular bones. For the pixel values of the profile $(h_1, h_2, \ldots, h_{100})$, the point closest to the starting point that satisfied $h_i - h_{i+1} < 0$ was considered as the candidate border point T_1. However, this T_1 may not be the true border point due to noise. Therefore, a search range of 20 pixels was set starting from T_1 toward the end of the profile. In this search range, the slope of the profile at each point, $S_i = h_i - h_{i+1}$ and the average slope S_{ave} were determined. Finally, the point closest to T_1 that satisfied $S_i > S_{\text{ave}}$ was selected as the border point T_2. The distance between the starting point and T_2 was considered as the cortical thickness for the profile. The average of 21 measurements on the right and left measurement locations was presented as the result.

The automated measurement results were compared with the manual measurement results by the dental radiologist. For the manual measurement, the dental radiologist placed lines corresponding to the width of cortical bone on both sides near the MF on the monitor. These lines were measured by use of Photoshop and considered the "gold standard" in this study. During the measurement, the cases were randomized and the diagnosis was not provided to the radiologist. The utility of the MCW for distinguishing between osteoporotic and control individuals was evaluated by use of the receiver operating characteristic (ROC) curve [15].

Results

Determination of the mandibular contours was largely successful for the measurement of MCWs in all cases by the visual assessment, and there was no processing error that could halt the MCW computation The average MCW of the control cases was 3.9 mm (SD = 0.79 mm), and that of the osteoporotic cases was 2.2 mm (SD = 0.62 mm). Figure 4 shows the box plots for 26 osteoporotic cases and 74 control cases. There was a statistically significant difference in

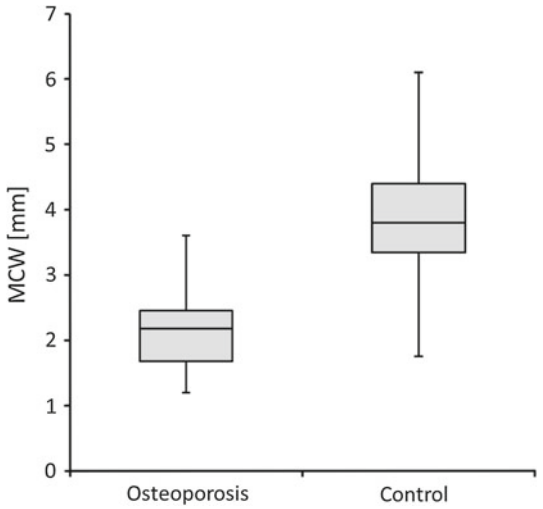

Fig. 4 Box plots showing the average MCWs and their ranges for the osteoporotic and control cases

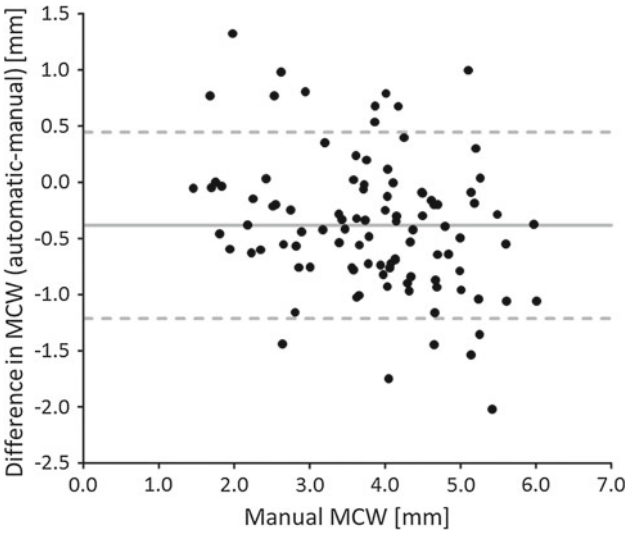

Fig. 5 Bland-Altman plot showing the relationship between the gold standard and the differences in automated and manual measurements for the 100 cases

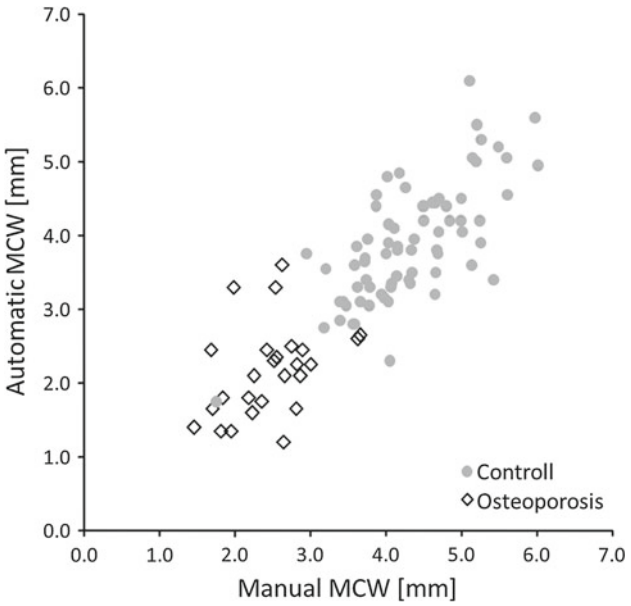

Fig. 6 Relationship between the gold standard MCWs and automatically determined MCWs

MCWs between the two groups based on the student's t-test ($p < 0.00001$).

The average MCWs for the osteoporotic and control cases by the manual measurements were 2.5 and 4.3 mm, respectively. In order to compare the measurement results with the manual measurement, Bland-Altman plot is presented in Fig. 5. Note that in this figure, the horizontal axis is the reference standard instead of the average [16]. The dashed lines specify the 95 % limits of agreement. It can be seen that although agreement between the two measurements is relatively good, the automatic measurements are, on average, slightly smaller than the manual measurements. In addition, there might be a trend that when the manual measurements are small, the automatic measurements are slightly larger, whereas when the manual measurements are large, the corresponding automatic measurements are slightly smaller.

Overall, the automatic measurements correlate well with the manual measurements, as shown in Fig. 6. The correlation coefficient between the gold standard MCWs and the automatic MCWs was 0.84. Areas under the ROC curves (AUC) for distinction between osteoporotic and control cases by the automatic and manual measurements were 0.96 and 0.98, respectively. There was no significant difference in AUC between the two ($p = 0.4$). Table 1 shows the sensitivity–specificity pairs at different threshold lengths. At the threshold of 3.0 mm, the sensitivity and specificity are 88.5 and 91.9 %, respectively.

Table 1 Sensitivity and specificity levels at different threshold lengths of MCWs

	Threshold = 2.7 mm	Threshold = 3.0 mm	Threshold = 3.5 mm
Sensitivity (%)	88.5	88.5	96.2
Specificity (%)	97.3	91.9	66.2

Discussion

We have developed a computerized scheme for automatically measuring MCWs on DPRs. By testing the proposed scheme on 100 cases including 26 DPRs of osteoporotic patients, a high correlation between the manual measurements and automatic measurements was observed. With the ROC analysis, the results indicated the comparable classification abilities for both measurements. At present, there seems to be no standard value of MCW in recommending patients for further examination. In previous clinical studies [3–5], the thresholds between 2.9 and 4.676 mm were applied. In other studies for computerized measurement [6–10], 3–4 mm or some unspecified values were used. Taguchi et al. have suggested the recommendation of DXA test for patients with MCW less than 3 mm based on the results of Japanese and European studies. As done in other studies, we presented the sensitivity and specificity levels at three threshold values including 3 mm, and the results are encouraging.

In some cases, however, MCWs were not measured accurately by the proposed method. There are two possible reasons for failures in the MCW measurement. A major reason was that the border between the cortical and trabecular bones was not detected accurately due to an indistinct margin. In some cases, it is very difficult to determine the endocortical margin even manually, as shown in Fig. 7a. Therefore, even when the lower mandibular edge is reasonably well detected (Fig. 7c), the border point was not determined accurately as

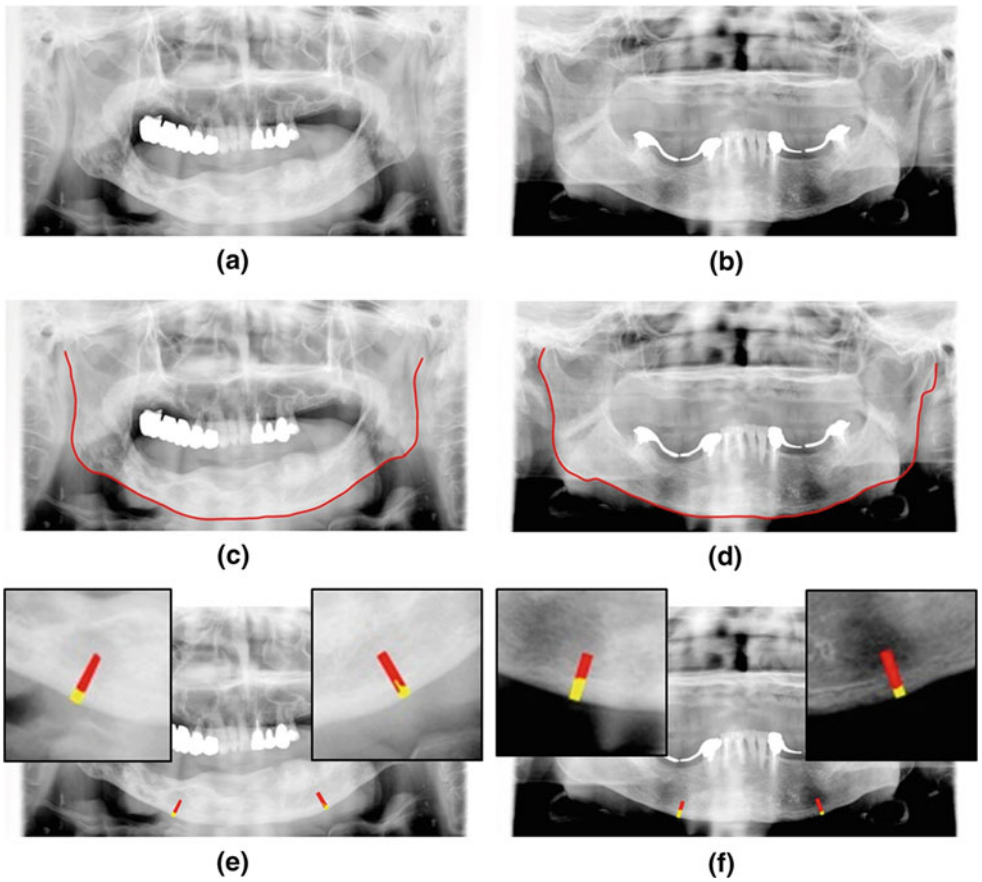

Fig. 7 Cases with MCW measurement failures due to indistinct endocortical margin (*left column*) and suboptimal selection of the measurement position (*right column*). **a**, **b** original image; **c**, **d** detected mandibular contour; **e**, **f** MCW measurement results

shown in Fig. 7e. Other reason could be due to the suboptimal selection of the measurement position as shown in Figs. 7b, f. By the proposed method, the detection of mandibular contour was relatively successful, especially the lower part between two angles. However, even when the contour detection was successful, as shown in Fig. 7d, the measurement position could be slightly shifted. It may be due to the individual variation in MF positions between the selected model and test cases, or the variation in the patient positioning. On the basis of these results, a new process to solve these problems may be required in the future.

Three osteoporotic cases were not classified correctly in our database. In this study, the classification was based only on the MCWs. Because the majority of osteoporotic patients are postmenopausal women, the classification accuracy could be improved by including the clinical information, such as age and gender [10]. An additional quantitative analysis on the roughness of cortical bones, which is often used in the clinical assessment of the disease progression, may improve the classification ability further. In one control case, MCW was remarkably smaller than the other control cases by both manual and automatic measurements. Although the reason for this is not clear, this patient may be considered as in potential osteoporotic condition.

In previous studies on MCW measurement, Arifin et al. [6] proposed the semiautomatic method by identifying the cortical margin. They reported the sensitivity and specificity of 88.0 and 58.7 %, respectively, on 100 cases including 25 cases with low BMD in lumbar spine. Roberts et al. [8] developed an automated scheme for measuring MCW by estimating the superior and inferior borders of cortical bones. When the method was applied to 663 cases including 140 osteoporotic cases, they achieved the sensitivity and specificity of 80.0 and 77.5 %, respectively. Our result cannot be compared with these results quantitatively due to different database used. Our fully automatic method uses a reference contour model to determine lower mandibular border trying to avoid the errors due to poor estimation of endocortical border. By using model, the MCW measurement positions under MF could be reliably identified in most cases.

Our study has several limitations. One is that the detailed evaluation of the proposed scheme was based on the proprietary dataset of 100 cases obtained with single imaging system which were also used for training. In order to reduce

bias, a leave-one-out test method was employed. Further evaluation is needed with a larger number of independent osteoporotic cases. Another limitation is that since most of DPRs used in this study were collected consecutively on the basis of the history of having DXA examination, there was a significant difference in age between osteoporotic and control groups (69.7 and 50.3, respectively; $p < 0.0001$). Because this study is our preliminary study to evaluate the methodology of MCW measurement and the number of cases is limited, all 100 cases were used. However, if 26 osteoporotic and 38 control cases with 50 years of age and older are used, the specificity becomes 89.5 % at the same sensitivity level of 88.5 % with 3 mm threshold. Usefulness of our proposed method in an age-matched case–control setting would be the subject of our future study.

Conclusion

A computerized scheme that measures the MCWs on DPRs was developed. Experimental results showed that the sensitivity and specificity for identifying osteoporotic patients were 88.5 and 97.3 %, respectively, with the threshold value of 2.7 mm. The result indicates that our proposed scheme has a potential to allow a secondary use of DPRs which were originally obtained for other purposes (generally dental diagnosis) to notify patients with a possible risk of osteoporosis and recommend a further examination. This was our preliminary study, and a multiclinic trial is under way to validate the usefulness of the proposed scheme.

Acknowledgments Authors are grateful to Asahi University Hospital staffs for their contribution in preparing image data. This research was supported in part by a Ministry of Education, Culture, Sports, Science and Technology (MEXT) Regional Innovation Strategy Support Program (City Area Type) in Southern Gifu Area, a Grant-in-Aid for Scientific Research on Innovative Areas, MEXT, Japan, and Strategic Information and Communications R&D Promotion Programme of the Ministry of Internal Affairs and Communications (MIC), Japan.

Conflict of interest This study was conducted by the collaboration of researchers at Gifu University, Asahi University, and Media Co., and partly supported by Japanese government research funding. There was no other financial support that would have inappropriately influenced our study.

References

1. Lane NE (2006) Epidemiology, etiology, and diagnosis of osteoporosis. Am J Obstet Gynecol 194:S3–S11
2. Yamamoto I (1999) Estimation of population of osteoporosis patients. Guideline on treatment of osteoporosis. Estimation based on results conforming to diagnostic criteria of Japan Soc. for Bone and Mineral Res. Osteoporos Jpn 7:10–11
3. Taguchi A (2010) Triage screening for osteoporosis in dental clinics using panorama radiographs. Oral Dis 16:316–327
4. Karayianni K, Homer K, Mitsea A, Berkas L, Mastoris M, Jacobs R et al (2007) Accuracy in osteoporosis diagnosis of a combination of mandibular cortical width measurement on dental panoramic radiographs and a clinical risk index(OSIRIS): the OSTEODENT project. Bone 40:223–229
5. Alman AC, Johnson LR, Calverley DC, Grunwald GK, Lezotte DC, Hokanson JE (2012) Diagnostic capabilities of fractal dimension and mandibular cortical width to identify men and women with decreased bone mineral density. Osteoporos Int 23(5):1631–1636
6. Arifin AZ, Asano A, Taguchi A, Nakamoto T, Ohtsuka M, Tsuda M et al (2006) Computer-aided system for measuring the mandibular cortical width on panoramic radiographs in identifying postmenopausal women with low bone mineral density. Osteoporos Int 17:753–759
7. Kavitha MS, Asano A, Taguchi A, Kurita T, Sanada M (2012) Diagnosis of osteoporosis from dental panoramic radiographs using the support vector machine method in a computer-aided diagnosis. BMC Med Imaging 12(1):1–11
8. Allen PD, Graham J, Farnell DJJ, Harrison EJ, Jacobs R, Nicopolou-Karayianni K et al (2007) Detecting reduced bone mineral density from dental radiographs using statistical shape models. IEEE Trans Inform Tech Biomed 11:601–610
9. Roberts MG, Graham J, Devlin H (2010) Improving the detection of osteoporosis from dental radiographs using active appearance models. In: Proceedings of IEEE international symposium on biomedical imaging, pp 440–443
10. Roberts MG, Yuan J, Graham J, Jacobs R, Devlin H (2011) Changes in mandibular cortical width measurements with age in men and women. Osteoporos Int 22:1915–1925
11. Matsumoto T, Hayashi T, Hara T, Katsumata A, Muramatsu C, Zhou X et al (2012) Automated scheme for measuring mandibular cortical thickness on dental panoramic radiographs for osteoporosis screening. Proc SPIE Med Imaging 8315:83152L1–83152L6
12. Canny J (1986) A computational approach to edge detection. IEEE Trans Patten Anal Mach Intell 8:679–698
13. Kirsch RA (1971) Computer determination of the constituent structure of biological images. Comput Biomed Res 4:1315–1328
14. Kass M, Witkin A, Terzopoulos D (1988) Snakes: Active contour models. Int J Comput Vis 1:321–331
15. Dorfman DD, Berbaum KS, Metz CE (1992) Receiver operating characteristic rating analysis: Generalization to the population of readers and patients with the jackknife method. Invest Radiol 27:723–731
16. Krouwer JS (2008) Why Bland-Altman plots should use X, not (Y+X)/2 when X is a reference method. Stat Med 27:778–780